2. Lecture 2. Adaptivity I: Design and Convergence of AFEM

Starting with a conforming mesh $\mathcal{T}_H$, the adaptive procedure AFEM consists of loops of the form

$$\boxed{\text{SOLVE} \to \text{ESTIMATE} \to \text{MARK} \to \text{REFINE}}$$

to produce the next conforming *nested* triangulation $\mathcal{T}_h$. The procedure SOLVE solves (1.15) for the discrete solution u_H. The procedure ESTIMATE determines the element indicators $\eta_H(T)$ and oscillation $\operatorname{osc}_H(T)$ for all elements $T \in \mathcal{T}_H$. Depending on their relative size, these quantities are later used by the procedure MARK to mark elements T, and thereby create a subset $\widehat{\mathcal{T}}_H$ of $\mathcal{T}_H$ of elements to be refined. Finally, procedure REFINE partitions those elements in $\widehat{\mathcal{T}}_H$ and a few more to maintain mesh conformity. These procedures are discussed in detail below. The theory started with Dörfler [21], but we follow the more recent developments [32, 34, 35].

2.1. Procedure ESTIMATE: A Posteriori Error Bounds.
In addition to $\mathcal{T}_H$, let $\mathcal{S}_H$ denote the set of interior faces (edges or sides) of the mesh $\mathcal{T}_H$. According to (1.17), we consider the *residual* $\mathcal{R} = \mathcal{R}(u_H) \in \mathbb{V}^*$ defined by

$$\mathcal{R}(u_H) := f + \operatorname{div}(\mathbf{A}\nabla u_H) - \mathbf{b} \cdot \nabla u_H - c\, u_H,$$

and its relation to the error $\mathcal{L}(u - u_H) = \mathcal{R}(u_H)$. In view of Lemma 1.5 it suffices to estimate $\|\mathcal{R}(u_H)\|_{\mathbb{V}^*}$. To this end, we set $e_H := u - u_H$ and integrate by parts $\mathcal{B}[e_H, v]$ elementwise to obtain the *error representation formula*

$$(2.1) \qquad \mathcal{B}[e_H, v] = \langle \mathcal{R}(u_h), v \rangle = \sum_{T \in \mathcal{T}_H} \int_T R_T(u_H) v + \sum_{S \in \mathcal{S}_H} \int_S J_S(u_H) v \qquad \forall\, v \in \mathbb{V},$$

where the *element residual* $R_T(u_H)$ and the *jump residual* $J_S(u_H)$ are defined as

$$(2.2) \qquad R_T(u_H) := f + \operatorname{div}(\mathbf{A}\nabla u_H) - \mathbf{b} \cdot \nabla u_H - c\, u_H \qquad \text{in } T \in \mathcal{T}_H,$$

$$(2.3) \qquad J_S(u_H) := -\mathbf{A}\nabla u_H^+ \cdot \nu^+ - \mathbf{A}\nabla u_H^- \cdot \nu^- := [\![\mathbf{A}\nabla u_H]\!]_S \cdot \nu_S \qquad \text{on } S \in \mathcal{S}_H,$$

where S is the common side of elements T^+ and T^- with unit outward normals ν^+ and ν^-, respectively, and $\nu_S = \nu^-$. Whenever convenient, we will use the abbreviations $R_T = R_T(u_H)$ and $J_S = J_S(u_H)$.

2.1.1. *Upper Bound.* For $T \in \mathcal{T}_H$ we define the *local error indicator* $\eta_H(T)$ by

$$(2.4) \qquad \eta_H(T)^2 := H_T^2 \|R_T(u_H)\|_{L^2(T)}^2 + \sum_{S \subset \partial T} H_S \|J_S(u_H)\|_{L^2(S)}^2.$$

Given a subset $\omega \subset \Omega$, we define the *error estimator* $\eta_H(\omega)$ by

$$\eta_H(\omega)^2 := \sum_{T \in \mathcal{T}_H,\, T \subset \omega} \eta_H(T)^2.$$

Hence, $\eta_H(\Omega)$ is the residual-type error estimator of Ω with respect to the mesh $\mathcal{T}_H$. This estimator is the simplest in the literature but not the most precise. We now find a first relation between $\eta_H(\Omega)$ and the energy error.

Lemma 2.1 (A Posteriori Upper Bound). *There exists a constant $C_1 > 0$ depending only on the shape regularity constant γ^*, and the coercivity and continuity constants $c_\mathcal{B}$ and $C_\mathcal{B}$ of $\mathcal{B}$, such that*

$$(2.5) \qquad \|u - u_H\|^2 \leq C_1 \eta_H(\Omega)^2.$$

Proof. With $\phi := e_H - I_H e_H$ we can write

$$
\begin{aligned}
\|e_H\|^2 = \mathcal{B}[e_H, e_H] &= \langle \mathcal{R}(u_H), e_H \rangle && \text{(definition (1.17) of } \mathcal{R}(u_H)) \\
&= \langle \mathcal{R}(u_H), \phi \rangle && \text{(Galerkin orthogonality (1.13))} \\
&= \sum_{T \in \mathcal{T}_H} \int_T R_T \phi + \sum_{S \in \mathcal{S}_H} \int_S J_S \phi && \text{(expression (2.1) of } \mathcal{R}) \\
&\leq \sum_{T \in \mathcal{T}_H} \|R_T\|_{L^2(T)} \|\phi\|_{L^2(T)} + \sum_{S \in \mathcal{S}_H} \|J_S\|_{L^2(S)} \|\phi\|_{L^2(S)} && \text{(Cauchy-Schwarz)}
\end{aligned}
$$

In view of the interpolation estimate (1.22), we have $\|\phi\|_{L^2(T)} \leq C H_T \|\nabla e_H\|_{L^2(N(T))}$ as well as

$$
\begin{aligned}
\sum_{T \in \mathcal{T}_H} \|R_T\|_{L^2(T)} \|\phi\|_{L^2(T)} &\leq C \sum_{T \in \mathcal{T}_H} \|H R_T\|_{L^2(T)} \|\nabla e_H\|_{L^2(N(T))} \\
&\leq C \Big(\sum_{T \in \mathcal{T}_H} \|H R_T\|_{L^2(T)}^2 \Big)^{1/2} \|e_H\|,
\end{aligned}
$$

where we have used the finite overlapping property of the neighborhoods $N(T)$ of elements $T \in \mathcal{T}_H$. On the other hand, we recall the scaled trace inequality for $S \in \mathcal{S}_H$ and element $T_S \in \mathcal{T}_H$ with side S

$$
\|\phi\|_{L^2(S)} \leq C H_S^{1/2} \|\nabla \phi\|_{L^2(T_S)} + C H_S^{-1/2} \|\phi\|_{L^2(T_S)}.
$$

This, in conjunction with (1.22), yields

$$
\begin{aligned}
\sum_{S \in \mathcal{S}_H} \|J_S\|_{L^2(S)} \|\phi\|_{L^2(S)} &\leq C \sum_{S \in \mathcal{S}_H} \|H^{1/2} J_S\|_{L^2(S)} \|\nabla e_H\|_{L^2(N(S))} \\
&\leq C \Big(\sum_{S \in \mathcal{S}_H} \|H^{1/2} J_S\|_{L^2(S)} \Big)^{1/2} \|e_H\|.
\end{aligned}
$$

Since we can always associate the side contributions by elements, we arrive at the asserted estimate. $\quad\square$

2.1.2. *Lower Bound.* Let $\overline{R_T} \in \mathbb{P}_{k-1}(T)$ be the L^2-projection of R_T, where $k \geq 1$ is the polynomial degree. We define the *oscillation* on the elements $T \in \mathcal{T}_H$ by

$$
\text{(2.6)} \qquad \text{osc}_H(T)^2 := H_T^2 \left\| R_T - \overline{R_T} \right\|_{L^2(T)}^2,
$$

and for a subset $\omega \subset \Omega$, we define

$$
\text{osc}_H(\omega)^2 := \sum_{T \in \mathcal{T}_H,\, T \subset \omega} \text{osc}_H(T)^2.
$$

We point out that osc_H is a convenient means to quantify information missed by the averaging process associated with the FEM. Using the explicit construction of Verfürth [1, 46] via bubble functions and positivity, and continuity of A, we can get a local lower bound of the error in terms of local indicators and oscillation. We point out that our construction deals with discrete bubble functions in a space $\mathbb{V}_h$ containing $\mathbb{V}_H$ and defined over a refinement of $\mathcal{T}_h$ of $\mathcal{T}_H$; this idea is due to Dörfler [21] and will be crucial later.

Lemma 2.2 (A Posteriori Lower Bound). *There exists a constant $C_2 > 0$, depending only on the shape regularity constant γ^*, C_B, and c_B, such that*

$$
\text{(2.7)} \qquad C_2 \eta_H(T)^2 \leq \|u - u_H\|_{H^1(\omega_T)}^2 + \text{osc}_H(\omega_T)^2,
$$

where the domain ω_T consists of all elements sharing at least a side with T.

Proof. We assume that ω_T for $T \in \mathcal{T}_H$ is refined in such a way that there is an interior node in each element in ω_T and each side of T. We also assume that the test function v in (2.1) is piecewise
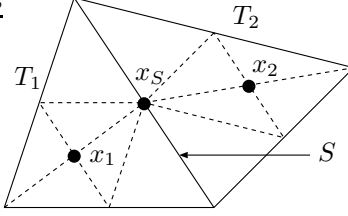
FIGURE 2.1. Example of a refined two-element patch $T_1 \cup T_2$ in two dimensions.

polynomial of degree $\leq k$ over the refinement of ω_T, namely $v \in \mathbb{V}_h$, and $\text{supp}(v) \subset \omega_T$. Note that (2.1) reads

$$(2.8) \qquad \mathcal{B}[e_H, v] = \sum_{T \in \mathcal{T}_H} \int_T \overline{R_T} v + \int_T (R_T - \overline{R_T}) v + \sum_{S \in \mathcal{S}_H} \int_S J_S \, v.$$
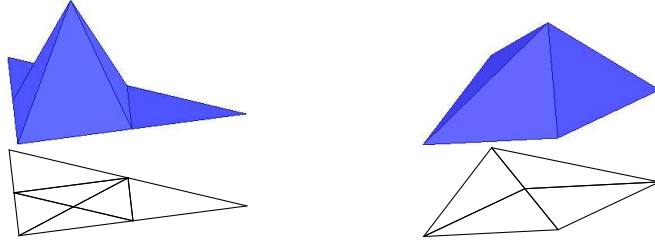

FIGURE 2.2. Discrete bubble functions ψ_1, ψ_S associated with the interior nodes x_1, x_S of Fig. 2.1 for polynomial degree $k = 1$.

We proceed in three steps.

1. *Interior Residual.* Let $T \in \mathcal{T}_H$, and let $x_T \in \mathcal{T}_h$ be an interior node of T. Let $\psi_T \in \mathbb{V}_h$ be a bubble function which satisfies $\psi_T(x_T) = 1$, vanishes on ∂T, and $0 \leq \psi_T \leq 1$; hence $\text{supp}(\psi_T) \subset T$. Since $\overline{R_T} \in \mathbb{P}_{k-1}(T)$ and $\psi_T > 0$ in a polyhedron of measure comparable with that of T, we have

$$C \left\| \overline{R_T} \right\|_{L^2(T)}^2 \leq \int_T \psi_T \, \overline{R_T}^2 = \int_T \overline{R_T}(\psi_T \, \overline{R_T}).$$

Since $v = \psi_T \overline{R_T}$ is a piecewise polynomial of degree $\leq k$ over $\mathcal{T}_h$, it is thus an admissible test function in (2.8) which vanishes outside T (and in particular on all $S \in \mathcal{S}_H$). Therefore

$$C \left\| \overline{R_T} \right\|_{L^2(T)}^2 \leq \mathcal{B}[e_H, \psi_T \overline{R_T}] + \int_T (\overline{R_T} - R_T) \psi_T \overline{R_T}$$
$$\leq C \left(H_T^{-1} \left\| e_H \right\|_{H^1(T)} + \left\| R_T - \overline{R_T} \right\|_{L^2(T)} \right) \left\| \overline{R_T} \right\|_{L^2(T)},$$

because of the inverse inequality $\|\nabla v\|_{L^2(T)} \leq C H_T^{-1} \|v\|_{L^2(T)}$. This, together with the triangle inequality, yields the desired estimate for $H_T^2 \|R_T\|_{L^2(T)}^2$:

$$(2.9) \qquad H_T^2 \|R_T\|_{L^2(T)}^2 \leq C \left(\|e_H\|_{H^1(T)}^2 + H_T^2 \left\| R_T - \overline{R_T} \right\|_{L^2(T)}^2 \right).$$

2. *Jump Residual.* Let $S \in \mathcal{S}_H$ be an interior side of $T_1 = T \in \mathcal{T}_H$, and let $T_2 \in \mathcal{T}_H$ be the other element sharing S. Let $x_S \in \mathcal{T}_h$ be an interior node of S. Let $\psi_S \in \mathbb{V}_h$ be a bubble function in $\omega_S := T_1 \cup T_2$ such that $\psi_S(x_S) = 1$, ψ_S vanishes on $\partial \omega_S$, and $0 \leq \psi_S \leq 1$; hence $\text{supp}(\psi_S) \subset \omega_S$.

Since u_H is continuous, then $[\![\nabla u_H]\!]_S$ is parallel to ν_S, i.e. $[\![\nabla u_H]\!]_S = j_S \, \nu_S$. Moreover, the coefficient matrix $\mathbf{A}(x)$ being continuous implies

$$J_S = \mathbf{A}(x) [\![\nabla u_H]\!]_S \cdot \nu_S = j_S \, \mathbf{A}(x)\nu_S \cdot \nu_S = a(x) \, j_S,$$

where $a(x) := \mathbf{A}(x)\nu_S \cdot \nu_S$ satisfies $0 < \underline{a}_S \le a(x) \le \overline{a}_S$ with $\underline{a}_S, \overline{a}_S$ the smallest and largest eigenvalues of $\mathbf{A}(x)$ on S. Consequently,

$$(2.10) \qquad \|J_S\|_{L^2(S)}^2 \le \overline{a}_S^2 \int_S j_S^2 \le C\overline{a}_S^2 \int_S j_S^2 \psi_S \le C\frac{\overline{a}_S^2}{\underline{a}_S} \int_S (j_S \, \psi_S)J_S,$$

where the second inequality follows from j_S being a polynomial and $\psi_S > 0$ in a polygon of measure comparable with that of S.

We now extend j_S to ω_S by first mapping to the reference element, next extending constantly along the normal to $\hat{S}$ and finally mapping back to ω_S. The resulting extension $E_h(j_S)$ is a piecewise polynomial of degree $\le n-1$ in ω_S so that $\psi_S E_h(j_S) \in \mathbb{V}_h$, and satisfies $\|\psi_S E_h(j_S)\|_{L^2(\omega_S)} \le CH_S^{1/2} \|j_S\|_{L^2(S)}$. Since $v = \psi_S E_h(j_S) \in \mathbb{V}_h$ is an admissible test function in (2.8) which vanishes on all sides of $\mathcal{S}_H$ but S, we arrive at

$$\int_S J_S(j_S\psi_S) = \mathcal{B}[e_H, v] - \int_{T_1} R_{T_1} \, v - \int_{T_2} R_{T_2} \, v$$
$$(2.11)$$
$$\le C \left(H_S^{-1/2} \|e_H\|_{H^1(\omega_S)} + H_S^{1/2} \sum_{i=1}^{2} \|R_{T_i}\|_{L^2(T_i)} \right) \|j_S\|_{L^2(S)} .$$

Therefore

$$(2.12) \qquad H_S \|J_S\|_{L^2(S)}^2 \le C \left(\|e_H\|_{H^1(\omega_S)}^2 + \sum_{i=1}^{2} H_{T_i}^2 \|R_{T_i}\|_{L^2(T_i)}^2 \right) .$$

3. *Final Estimate.* To remove the interior residual from the right hand side of (2.12) we observe that both T_1 and T_2 contain an interior node of $\mathcal{T}_h$. Hence, (2.9) implies

$$(2.13) \qquad H_S \|J_S\|_{L^2(S)}^2 \le C \left(\|\varepsilon_H\|_{H^1(\omega_S)}^2 + \sum_{i=1}^{2} H_{T_i}^2 \left\|R_{T_i} - \overline{R_{T_i}}\right\|_{L^2(T_i)}^2 \right) .$$

The asserted estimate for $\eta_H(T)^2$ is thus obtained by adding this bound to (2.9). The constant C depends on the shape regularity constant γ^* and the ratio $\overline{a}_S^2/\underline{a}_S$ of largest and smallest eigenvalues of $\mathbf{A}(x)$ for $x \in S$. $\qquad\square$

Remark 2.3 (Equidistribution). We see from (2.7) that if the oscillation $\mathrm{osc}_H(\omega_T)$ is small compared to the indicator $\eta_H(T)$, then the size of the indicator $\eta_H(T)$ will give reliable information about the size of the error $\|u - u_H\|_{H^1(\omega_T)}$. This explains why refining elements with large indicators usually tends to equi-distribute the errors which, according to Example 1.9, is an ultimate goal of adaptivity. This idea is employed by the procedure MARK of §2.2.

Remark 2.4 (Positivity). The use of $\mathbf{A}(x)$ being positive definite in (2.10) avoids having oscillation terms on S. This comes at the expense of a constant depending on $\overline{a}_S^2/\underline{a}_S$. If we were to proceed in the usual manner, as in [1, 37, 46], we would end up with an oscillation of the form

$$H_S^{1/2} \|(\mathbf{A}(x) - \mathbf{A}(x_S)) [\![\nabla u_H]\!]_S \cdot \nu_S\|_{L^2(S)} = H_S^{1/2} \|(a(x) - a(x_S))j_S\|_{L^2(S)}$$
$$\le CH_S^{3/2} \|\mathbf{A}\|_{W_\infty^1(S)} \|j_S\|_{L^2(S)}$$
$$\le CH_S \left\|H_S^{1/2} J_S\right\|_{L^2(S)},$$

where $C > 0$ also depends on the ratio $\overline{a}_S/\underline{a}_S$ dictated by the variation of $a(x)$ on S. This oscillation can be absorbed into the term $H_S^{1/2} \|J_S\|_{L^2(S)}$ provided that the meshsize H_S is sufficiently small; see [37]. We do not need this assumption in our present discussion.

Remark 2.5 (Continuity of **A**). The continuity of **A** is instrumental in avoiding jump oscillations which in turn makes computations simpler. However, jump oscillations cannot be avoided when **A** exhibits discontinuities across inter-element boundaries of the initial mesh. We get instead of (2.13)

$$(2.14) \qquad CH_S \|J_S\|_{L^2(S)}^2 \le \|\varepsilon_H\|_{H^1(\omega_S)}^2 + \sum_{i=1}^2 H_{T_i}^2 \|R_{T_i} - \overline{R_{T_i}}\|_{L^2(T_i)}^2 + H_S \|J_S - \overline{J_S}\|_{L^2(S)}^2,$$

where $\overline{J_S}$ is the L^2-projection of J_S onto $\mathbb{P}_{k-1}(S)$. To obtain estimate (2.14) we proceed as follows. Starting from a polynomial $\overline{J_S}$, we get an estimate similar to that of (2.10)

$$(2.15) \qquad C \left\|\overline{J_S}\right\|_{L^2(S)}^2 \le \int_S \psi_S \overline{J_S}^2 = \int_S J_S(\psi_S \overline{J_S}) + \int_S (\overline{J_S} - J_S)(\psi_S \overline{J_S}).$$

In contrast to (2.10), we see that the oscillation term $(\overline{J_S} - J_S)$ cannot be avoided when **A** has a discontinuity across S. We estimate the first term on the right hand side of (2.15) exactly as we have argued with (2.11) and thereby arrive at

$$\int_S J_S(\overline{J_S}\psi_S) \le C \left(H_S^{-1/2} \|\varepsilon_H\|_{H^1_S(\omega_S)} + H_S^{1/2} \sum_{i=1}^2 \|R_{T_i}\|_{L^2(T_i)} \right) \left\|\overline{J_S}\right\|_{L^2(S)}.$$

This and a further estimate of the second term on the right hand side of (2.15), yield

$$H_S \left\|\overline{J_S}\right\|_{L^2(S)}^2 \le C \left(\|\varepsilon_H\|_{H^1(\omega_S)}^2 + \sum_{i=1}^2 H_{T_i}^2 \|R_{T_i}\|_{L^2(T_i)}^2 + H_S \left\|J_S - \overline{J_S}\right\|_{L^2(S)}^2 \right),$$

whence the assertion (2.14) follows using triangle inequality for $\|J_S\|_{L^2(S)}$. Combining with (2.9), we deduce an estimate for $\eta_H(T)$ similar to (2.7), namely,

$$\eta_H(T)^2 \le C \left(\|\varepsilon_H\|_{H^1(\omega_T)}^2 + \mathrm{osc}_H(\omega_T)^2 \right),$$

with the new oscillation term involving jumps on interior sides

$$(2.16) \qquad \mathrm{osc}_H(T)^2 := H_T^2 \left\|R_T - \overline{R_T}\right\|_{L^2(T)}^2 + \sum_{S \subset \partial T} H_S \left\|J_S - \overline{J_S}\right\|_{L^2(S)}^2.$$

For a given mesh $\mathcal{T}_H$ and discrete solution u_H, along with input data $\mathbf{A}, \mathbf{b}, c$ and f, the procedure ESTIMATE computes element indicators $\eta_H(T)$ and oscillations $\mathrm{osc}_H(T)$ for all $T \in \mathcal{T}_H$ according to (2.4) and (2.6):

$$\boxed{\{\eta_H(T), \mathrm{osc}_H(T)\}_{T \in \mathcal{T}_H} = \mathsf{ESTIMATE}(\mathcal{T}_H, u_H, \mathbf{A}, \mathbf{b}, c, f)}$$

2.2. Procedure MARK. Our goal is to devise a marking procedure, namely to identify a subset $\widehat{\mathcal{T}}_H$ of the mesh $\mathcal{T}_H$ such that after refining, both error and oscillation will be reduced. This is achieved with two marking strategies as follows.

The Marking Strategy E, also called bulk-chasing, was introduced by Dörfler [21]:

> `Marking Strategy E` : Given a parameter $0 < \theta_E < 1$, construct a *minimal* subset $\widehat{\mathcal{T}}_H$ of $\mathcal{T}_H$ such that
>
> $$(2.17) \qquad\qquad \sum_{T \in \widehat{\mathcal{T}}_H} \eta_H(T)^2 \ge \theta_E^2 \eta_H(\Omega)^2,$$
>
> and mark all elements in $\widehat{\mathcal{T}}_H$ for refinement.

We will see later that Marking Strategy E guarantees error reduction in the absence of oscillation terms. Since the latter account for information missed by the averaging process associated with the finite element method, we need a separate procedure to guarantee oscillation reduction.

This procedure was introduced by Morin et al. [34, 35] as a separate means for reducing oscillation:

> `Marking Strategy O` : Given a parameter $0 < \theta_0 < 1$ and the subset $\widehat{\mathcal{T}}_H \subset \mathcal{T}_H$ produced by Marking Strategy E, enlarge $\widehat{\mathcal{T}}_H$ to a *minimal* set such that
>
> $$(2.18) \qquad \sum_{T \in \widehat{\mathcal{T}}_H} \mathrm{osc}_H(T)^2 \geq \theta_0^2 \mathrm{osc}_H(\Omega)^2,$$
>
> and mark all elements in $\widehat{\mathcal{T}}_H$ for refinement.

Given a mesh $\mathcal{T}_H$ and all information about the local error indicators $\eta_H(T)$, and oscillation $\mathrm{osc}_H(T)$, together with user parameters θ and $\hat{\theta}$, MARK generates a subset $\widehat{\mathcal{T}}_H$ of $\mathcal{T}_H$

$$\widehat{\mathcal{T}}_H = \mathsf{MARK}(\theta_E, \theta_0 \; ; \; \mathcal{T}_H, \{\eta_H(T), \mathrm{osc}_H(T)\}_{T \in \mathcal{T}_H})$$

2.3. **Procedure REFINE and AFEM.** The following Interior Node Property, due to Morin et al [34, 35], is known to be necessary for error and oscillation reduction:

> `Interior Node Property` : Refine each marked element $T \in \widehat{\mathcal{T}}_H$ to obtain a new mesh $\mathcal{T}_h$ compatible with $\mathcal{T}_H$ such that
>
> T and the $d+1$ adjacent elements $T' \in \mathcal{T}_H$ of T, as well as their common sides, contain a node of the finer mesh $\mathcal{T}_h$ in their interior.

In addition to the Interior Node Property, we assume that the refinement is done in such a way that the new mesh $\mathcal{T}_h$ is conforming, which guarantees that both $\mathcal{T}_H$ and $\mathcal{T}_h$ are nested. This can be achieved by repeated bisection (see Figure 2.3).
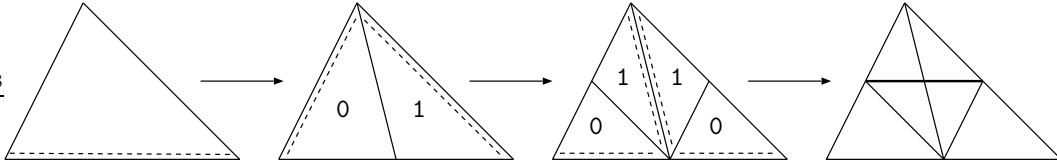
PSfrag replacements

FIGURE 2.3. Refinement of triangles in two dimensions by newest-vertex bisection. Dashed lines indicate the refinement edges, which are sides opposite to the most recently created nodes.

Creating interior nodes is rather easy in two dimensions. First, elements are marked for two bisections and then refined. This already produces a node at the midpoint of each edge. Second, the two grandchildren with index `1` are bisected once more. The whole refinement process is shown in Figure 2.3. The first refinement step may, as usual, involve surrounding elements which are not marked. This is an inevitable effect in order to preserve mesh conformity. The second refinement step is *local* in that it involves only the two grandchildren with index `1` and does not spread outside them.

In three dimensions it is impossible to perform the second step by dealing only with children of the original tetrahedron. The first step consists of three bisections. In order to obtain the interior nodes, the second step consists of marking some sub-tetrahedra for two or three additional bisections. This has the spreading effect of creating additional nodes in the edges of the original tetrahedron. For the implementation, we do not split the refinement into two steps, but rather mark a tetrahedron for six bisections which are performed in one step. This creates an interior node in the tetrahedron and interior nodes in all the element faces.

With this property, we have a reduction factor $\gamma_0 < 1$ of element size, i.e. if $T \in \mathcal{T}_h$ is obtained by refining $T' \in \widehat{\mathcal{T}}_H$, then $h_T \leq \gamma_0 H_{T'}$. In $d = 2$ with triangular elements, 3 newest bisections yield $\gamma_0 \leq 1/2$.

Given a mesh $\mathcal{T}_H$ and a marked set $\widehat{\mathcal{T}}_H$, REFINE constructs a conforming refinement $\mathcal{T}_h$ satisfying the Interior Node Property:

$$\boxed{\mathcal{T}_h = \mathsf{REFINE}(\mathcal{T}_H, \widehat{\mathcal{T}}_H)}$$

Given parameters θ_E and θ_0 according to Marking Strategies E and O, the adaptive algorithm AFEM consists of the loops of procedures SOLVE, ESTIMATE, MARK, and REFINE as follows:

AFEM

Choose parameters $0 < \theta_E, \theta_0 < 1$.
   (1) Pick an initial mesh $\mathcal{T}_0$, initial guest $u_{-1} = 0$, and set $k = 0$.
   (2) $u_k = \mathsf{SOLVE}(\mathcal{T}_k, u_{k-1}, \mathbf{A}, \mathbf{b}, c, f)$.
   (3) $\{\eta_k(T), \mathrm{osc}_k(T)\}_{T \in \mathcal{T}_k} = \mathsf{ESTIMATE}(\mathcal{T}_k, u_k, \mathbf{A}, \mathbf{b}, c, f))$.
   (4) $\widehat{\mathcal{T}}_k = \mathsf{MARK}(\theta, \hat{\theta} \; ; \; \mathcal{T}_k, \{\eta_k(T), \mathrm{osc}_k(T)\}_{T \in \mathcal{T}_k})$.
   (5) $\mathcal{T}_{k+1} = \mathsf{REFINE}(\mathcal{T}_k, \widehat{\mathcal{T}}_k)$.
   (6) Set $k = k + 1$ and go to Step 2.

2.4. **Error and Oscillation Reduction.** To shed light on the ingredients for convergence of AFEM, we discuss three examples. They show the significance of the Interior Node Property in reducing both error and oscillation. We consider the simplest scenario, thereby following [34, 35], and assume that $\mathbf{A}$ is piecewise constant (but possibly discontinuous) and that both $\mathbf{b}$ and c vanish. The resulting operator $\mathcal{L}$ reads

$$(2.19) \qquad\qquad \mathcal{L}u = -\,\mathrm{div}(\mathbf{A}\nabla u) = f,$$

and the corresponding oscillation merely depends on data

$$(2.20) \qquad\qquad \mathrm{osc}_H^2 = \sum_{T \in \mathcal{T}_H} H_T^2 \|f - \bar{f}_T\|_{L^2(T)}^2.$$

Example 2.6 (Interior Node 1). This example shows the necessity of creating an interior node inside each refined triangle. Consider problem (1.3)-(1.4) with $\mathbf{A} = \mathbf{I}$, $f \equiv 1$, and $\Omega = (0,1) \times (0,1)$. Let $\left\{(0,0), (1,0), (1,1), (0,1), (\frac{1}{2}, \frac{1}{2})\right\}$ be the set of vertices of $\mathcal{T}_0$ (see Figure 2.4-left).
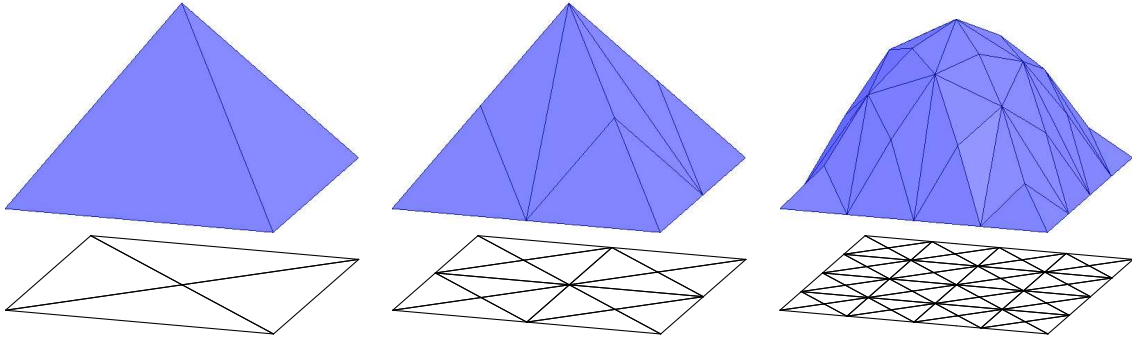

FIGURE 2.4. Example 2.6: Finite element solutions u_0, u_1, u_2 for 3 consecutive meshes $\mathcal{T}_0, \mathcal{T}_1, \mathcal{T}_2$ obtained with 2 bisection steps. The triangles of $\mathcal{T}_1$ do not have interior nodes but those of $\mathcal{T}_2$ do, thereby yielding $u_1 = u_2 = \frac{1}{12}\phi_1 \neq u_3$.

Let ϕ_1 be the nodal basis function of $\mathbb{V}_0$ that corresponds to the node $(\frac{1}{2}, \frac{1}{2})$. Then, it is easily seen that the finite element solution u_0 is $u_0 = \frac{1}{12}\phi_1$. Let $\mathcal{T}_1$ be the grid obtained from $\mathcal{T}_0$ by performing two bisections on each triangle of $\mathcal{T}_0$ using the newest-vertex bisection and assuming that $(\frac{1}{2}, \frac{1}{2})$ is the newest vertex on the initial grid (see Figure 2.4-middle). This is the standard refinement 2-step

bisection [21], and does not lead to an interior node in the refined elements. Then we get a set of 5 nodes, and the finite element solution u_1 on $\mathcal{T}_1$ solves a simple 5×5 system which satisfies $u_1 = u_0$, as can be seen in Figure 2.4. Since $u - u_1 = u - u_0$, we conclude that without one interior node in at least one triangle, no error reduction is obtained even when $\mathrm{osc}_0 = 0$ and $\|u - u_0\|_\Omega > 0$. The presence of interior nodes (with respect to $\mathcal{T}_0$) in the refinement $\mathcal{T}_2$ of $\mathcal{T}_1$ yields a change of solution values (see Figure 2.4-right).

Example 2.7 (Interior Node 2)**.** At first sight, it may seem that the situation of Example 2.6 may occur only at the first refinement step. This example shows that such a situation can also happen at any refinement step n.

Fix $n \in \mathbb{N}_0$ and consider (1.3) with $\mathbf{A} = \mathbf{I}$, $\Omega = (0,1)^2$, and f given by

$$f(x) = \begin{cases} 1 & \text{if } x \in (i\,2^{-n}, (i+1)\,2^{-n}) \times (j\,2^{-n}, (j+1)\,2^{-n}) \text{ and } i+j \text{ odd} \\ -1 & \text{otherwise;} \end{cases}$$

see Figure 2.5. Then, if we start with $\mathcal{T}_0$ equal to the grid $\mathcal{T}_0$ of Example 2.6, and ϕ_1 also as in Example 2.6, we have that ϕ_1 is orthogonal to f and consequently $u_0 \equiv 0$. If we now define recursively $\mathcal{T}_{k+1}$, $k = 0, 1, \ldots$ as the grid that results from $\mathcal{T}_k$ by performing two newest-vertex bisections on every triangle (see Figure 2.5), we will have $u_k \equiv 0$ for $k = 0, 1, \ldots, n-1$, due to the fact that f is orthogonal to the basis functions of $\mathcal{T}_k$ for $k = 0, 1, \ldots, n-1$.
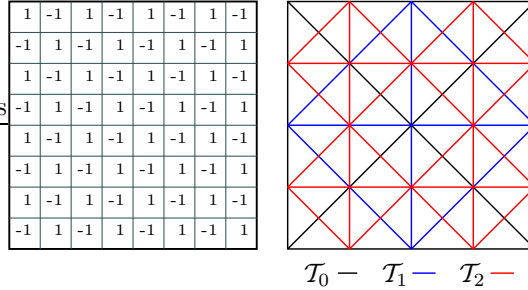

FIGURE 2.5. Example 2.7: Checkerboard function f for $n = 3$ (left), and grids $\mathcal{T}_k$ for $k = 0, 1, 2$ (right).
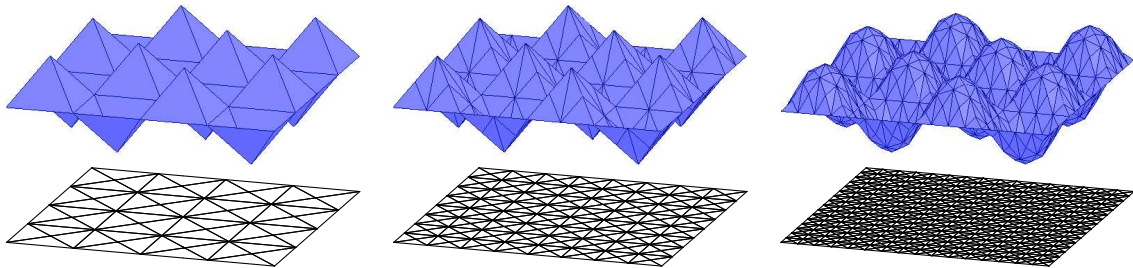

FIGURE 2.6. Example 2.7: Finite element solutions u_2, u_3, u_4 and meshes $\mathcal{T}_2, \mathcal{T}_3, \mathcal{T}_4$ with $n = 2$. Since $u_2 = u_3 \neq u_4$, error reduction may fail to hold at any adaptive loop not just at the first one.

For $k = n$ the solution u_n will not be zero anymore, but it will be zero along the lines where f changes sign due to the symmetry of the problem, and the same will happen with u_{n+1} (see Figure 2.6). Then, if we observe u_n and u_{n+1} in a fixed square where f is constant, they behave exactly as u_0 and u_1 do in Example 2.6, and consequently $u_n = u_{n+1}$, which means that the error does not decrease, even when the oscillation osc_n is zero. Figure 2.6 depicts this situation.

Example 2.8 (Data Oscillation)**.** This example shows that if the data oscillation osc_H is not small, then, even introducing an interior node on all elements, the error may not decrease. To see this, consider Example 2.7 for some fixed large $n \in \mathbb{N}_0$. Observe now that if we obtain $\mathcal{T}_{k+1}$ by performing *three* bisections on all the elements of $\mathcal{T}_k$, then three new nodes are created on the edge opposite to the newest vertex in addition to an interior node per element (see Figure 2.7). Even though this refinement is stronger than required by the Interior Node Property in each step, the solutions, u_k will all be zero for $k < 2n/3$.

PSfrag replacements

$\mathcal{T}_0$ — $\mathcal{T}_1$ — $\mathcal{T}_1$ — $\mathcal{T}_2$ —
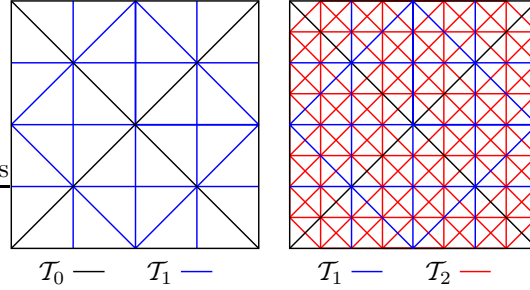
FIGURE 2.7. Resulting grid $\mathcal{T}_1$ (left) and $\mathcal{T}_2$ (right) after performing three bisections on each element of $\mathcal{T}_0$ and $\mathcal{T}_1$, respectively.

We conclude from Examples 2.6 and 2.7 that the interior node is necessary to obtain an error decrease, and from Example 2.8 that this may not be sufficient if the mesh does not resolve oscillation of data. Therefore, in order to obtain an *asymptotically convergent* sequence of discrete solutions, we must readjust the mesh to resolve osc_H according to a decreasing tolerance.

We next quantify to effect of the Interior Node Property for both error and oscillation reduction. We start with a simple result relating two consecutive discrete solutions on an element that has been refined.

Lemma 2.9 (Local Lower Bound for $u_h - u_H$)**.** *Let $C_2 > 0$ be the constant of Lemma 2.2. Then*

$$(2.21) \qquad C_2 \eta_H(T)^2 \leq \|u_h - u_H\|^2_{H^1(\omega_T)} + \text{osc}_H(\omega_T)^2 \qquad \forall\, T \in \widehat{\mathcal{T}}_H.$$

Proof. Since $\mathcal{B}[u - u_h, v] = 0$ for $v \in \mathbb{V}_h$, we have

$$\mathcal{B}[u - u_H, v] = \mathcal{B}[u_h - u_H, v] \qquad \forall\, v \in \mathbb{V}_h.$$

We now observe that the bubble functions in the proof of Lemma 2.2 are in $\mathbb{V}_h$. Therefore, the assertion follows as in Lemma 2.2. $\square$

We realize that the local energy error between consecutive discrete solutions is bounded below by the local indicators for elements in the marked set $\widehat{\mathcal{T}}_H$, provided the oscillation term is sufficiently small relative to the energy error.

On the other hand, we now prove that the oscillation reduces with a factor $\rho < 1$. The first lemma considers the worst scenario situation of f just in $L^2(\Omega)$, whereas the second lemma addresses the case of f piecewise smooth.

Lemma 2.10 (Data Oscillation Reduction 1)**.** *Let $0 < \gamma_0 < 1$ be the reduction factor of element size associated with one refinement step of REFINE. Given $0 < \theta_0 < 1$, let $\rho := (1 - (1 - \gamma_0^2)\theta_0^2)^{1/2}$. Let $\widehat{\mathcal{T}}_H$ be a subset of $\mathcal{T}_H$ satisfying Marking Strategy O. If $\mathcal{T}_h$ is generated by REFINE from $\mathcal{T}_H$, then the following data oscillation reduction occurs:*

$$(2.22) \qquad\qquad\qquad osc_h \leq \rho\, osc_H.$$

Proof. Let $T \in \mathcal{T}_h$ be an element contained in $\hat{T} \in \widehat{\mathcal{T}}_H$. Since $\bar{f}_T$ is the L^2-projection of f onto $\mathbb{P}_{k-1}(T)$, for instance $\bar{f}_T = |T|^{-1} \int_T f$ for $k = 1$, we have

$$\|f - \bar{f}_T\|_{L^2(T)} \le \|f - \bar{f}_{\hat{T}}\|_{L^2(T)}.$$

Since $h_T \le \gamma_0 h_{\hat{T}}$, we discover that

$$
\begin{aligned}
\mathrm{osc}_h^2 &= \sum_{T \in \mathcal{T}_h} h_T^2 \|f - \bar{f}_T\|_{L^2(T)}^2 \\
&\le \gamma_0^2 \sum_{\hat{T} \in \widehat{\mathcal{T}}_H} h_{\hat{T}}^2 \|f - \bar{f}_{\hat{T}}\|_{L^2(\hat{T})}^2 + \sum_{T \in \mathcal{T}_H \setminus \widehat{\mathcal{T}}_H} h_T^2 \|f - \bar{f}_T\|_{L^2(T)}^2 \\
&= (\gamma_0^2 - 1)\mathrm{osc}_H^2 + \mathrm{osc}_H^2 \le \rho^2 \mathrm{osc}_H^2.
\end{aligned}
$$

$\square$

2.5. **Convergence of AFEM.** We prove convergence of AFEM under the simplifying assumptions on the coefficients of section 2.4, following [34, 35]. We will consider the general case in Lecture 3.

It is crucial for convergence to be able to link two consecutive discrete solutions $u_H \in \mathbb{V}_H$ and $u_h \in \mathbb{V}_h$. This is easy to do for the energy norm due to Lemma 2.11, but not for any other norm.

Lemma 2.11 (Orthogonality). *If $\mathbb{V}_H \subset \mathbb{V}_h$, then the following relation holds*

$$(2.23) \qquad \|u - u_H\|^2 = \|u - u_h\|^2 + \|u_h - u_H\|^2.$$

Proof. The bilinear form $\mathcal{B}$, being symmetric, induces a scalar product in $\mathbb{V}$. By Galerkin orthogonality, $\mathcal{B}[e_h, v] = 0$ for all $v \in \mathbb{V}_h$, whence $u_h - u_H \in \mathbb{V}_h$ is perpendicular to $u - u_h$. Therefore, since $u - u_H = (u - u_h) + (u_h - u_H)$, the assertion (2.23) follows from the Pythagoras theorem $\square$

This resul reveals the monotonicity property $\|u - u_h\| \le \|u - u_H\|$ regardless of the strengh of the refinement leading from $\mathcal{T}_H$ to $\mathcal{T}_h$. To enforce a strick error reduction we need to make sure that $\|u_h - u_H\|$ is at least a fixed proportion of $\|u - u_H\|$. We do this next upon quantifying the effect of MARK and REFINE on error reduction. In particular, we show the compound effect of the Marking Strategy E with the Interior Node Property.

Theorem 2.12 (Error Reduction). *Given a triangulation $\mathcal{T}_H$ and discrete solution u_H, let $\widehat{\mathcal{T}}_H$ be generated by MARK and let $\mathcal{T}_h$ be a conforming refinement of $\mathcal{T}_H$ generated by REFINE. Then there exists a constant $0 < \alpha < 1$, depending only on the minimum angle, θ_E, C_B, and c_B, such that the solution u_h on the mesh $\mathcal{T}_h$ satisfies*

$$\|u - u_h\| \le \alpha \|u - u_H\| + osc_H^2.$$

Proof. We first derive a lower bound for $\|u_h - u_H\|$. By Lemma 2.9 and Marking Strategy E we have

$$
\begin{aligned}
C_2 \theta_E^2 \eta_H^2 &\le C_2 \sum_{T \in \widehat{\mathcal{T}}_H} \eta_H(T)^2 \\
&\le \sum_{T \in \widehat{\mathcal{T}}_H} \|u_h - u_H\|_{H^1(\omega_T)}^2 + \mathrm{osc}_H(\omega_T)^2 \\
&\le D \|u_h - u_H\|^2 + D\mathrm{osc}_H^2,
\end{aligned}
$$

where $D := d + 2$ accounts for the overlap of sets ω_T. Hence, since $\|u - u_H\|^2 \le C_1 \eta_H^2$ in light of Lemma 2.1,

$$\|u_h - u_H\|^2 \ge \frac{\theta_E^2 C_2}{D} \eta_H^2 - \mathrm{osc}_H^2 \ge \frac{\theta_E^2 C_2}{DC_1} \|u - u_H\|^2 - \mathrm{osc}_H^2$$

Cobining this with Lemma (2.11), we obtain

$$\|u - u_h\|^2 = \|u - u_H\|^2 - \|u_h - u_H\|^2$$

$$\leq \|u - u_H\|^2 \left(1 - \frac{\theta_E^2 C_2}{DC_1}\right) + \mathrm{osc}_H^2$$

This proves the assertion with $\alpha^2 = 1 - \frac{\theta_E^2 C_2}{DC_1}$. $\hfill\square$

Theorem 2.12 shows that the energy error decreases provided that oscillation decreases separately. The latter is provided by Lemma 2.10. We point out though that we do not prove a geometric decrease of the error but that rather that it is dominated by a geometric sequence.

Theorem 2.13 (Convergence). *Let $0 < \theta_E, \theta_0 < 1$ be the parameters of MARK. Let $0 < \alpha < 1$ be given by Theorem 2.12 and $0 < \rho < 1$ by Lemma 2.10. Let $\alpha_0 := \max(\alpha, \rho)$. Then, for every β such that $\alpha_0 < \beta < 1$, the sequence $\{u_k\}_{k \in \mathbb{N}_0}$ of finite element solutions produced by AFEM satisfies*

(2.24) $$\|u - u_k\|_{\Omega} \leq C_0 \, \beta^k,$$

with

$$C_0 := \|e_0\| + \frac{1}{\beta - \alpha_0} osc_0.$$

Proof. We first apply Lemma 2.10 recursively to get

$$\mathrm{osc}_k \leq \rho \, \mathrm{osc}_{k-1} \leq \cdots \leq \rho^k \mathrm{osc}_0.$$

We then set $e_k := \|u - u_k\|$, and utilize Theorem 2.12 to deduce

$$e_{k+1} \leq \alpha e_k + \mathrm{osc}_k \leq \alpha e_k + \rho^k \mathrm{osc}_0,$$

which by recursion implies

(2.25) $$e_{k+1} \leq \alpha^{k+1} e_0 + \mathrm{osc}_0 \sum_{j=0}^{k} \alpha^j \rho^{k-j}.$$

Since $\alpha \leq \alpha_0$ and $\rho < \beta$, we obtain the estimate

$$\sum_{j=0}^{k} \alpha^j \rho^{k-j} \leq \beta^k \sum_{j=0}^{k} \left(\frac{\alpha_0}{\beta}\right)^j \leq \beta^k \frac{1}{1 - \frac{\alpha_0}{\beta}} = \beta^{k+1} \frac{1}{\beta - \alpha_0},$$

from which the assertion follows immediately. $\hfill\square$

2.6. **Numerical Experiments.** In this section we present two examples taken from [34, 35]. The purpose of the simulations is to verify experimentally the optimal performance of AFEM. We monitor the error decay in terms of degrees of freedom N for polynomial degree $k = 1$, and observe the optimal rate $N^{-1/2}$. The experiments were implemented within the finite element toolbox ALBERTA [43].

2.6.1. *Example: Discontinuous coefficients.* We consider the Example 1.3 due to Kellogg [29].   In
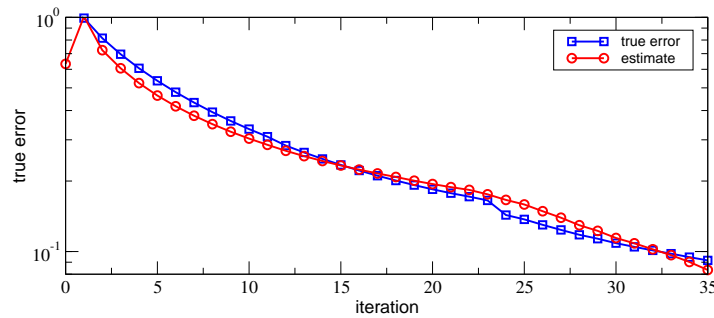

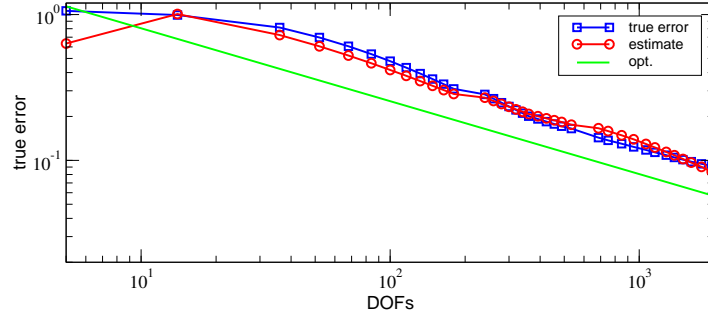FIGURE 2.8. Example 2.6.1: Error reduction: estimate and true error.

FIGURE 2.9. Example 2.6.1: Quasioptimality of AFEM: estimate and true error. The optimal decay is indicated by the green line with slope $-1/2$.

TABLE 2.1. Example 2.6.2: Total number and number of marked elements per iteration in two dimensions (left) and three dimensions (right): est.: marked elements due to error estimator, osc.: *additionally* marked elements to data oscillation.

iter.	elements	est.	osc.
0	4	8	0
1	64	16	16
2	704	56	8
3	2256	80	0
4	4208	96	8
5	6624	112	24
6	8752	344	0
7	17512	432	0
8	28368	608	0
9	42896	768	16
10	60216	2192	0
11	113040	2296	24
12	160592	3816	24

iter.	elements	est.	osc.
0	6	6	0
1	384	48	0
2	7776	48	48
3	15936	576	0
4	112320	5040	0
5	860592	5136	720
6	1693536	30144	0

Figures 2.8-2.9 we see the same behavior of the true error $\|e_k\|_\Omega$ and the estimator η_k scaled by the factor 0.05. Figure 2.9 demonstrates that the grids and associated numerical complexity are quasi-optimal: $\|e_k\|_\Omega = C \operatorname{DOFs}(k)^{-1/2}$ is valid asymptotically (the performance of an optimal method is again indicated by the additional green straight line).

For this problem the grid is highly graded at the origin. It is worth realizing the strength of the singularity at hand in Figure 2.10. We see a mesh with less than 2000 nodes and three zooms at the origin, each obtained with a magnifying factor 10^3, and yet exhibiting a rather strong grading. This is also reflected in Figure 2.11, which depicts the graph of the discrete solution over the underlying mesh: the solution is flatter in the quadrants with $a \approx 161$ although the grid is finer, which accounts for the presence of a in the energy norm. This picture was created using the graphics package GRAPE [27].

2.6.2. *Example: Variable Source.* In Example 2.6.1 the source term is constant. It is our purpose now to examine the effect of data oscillation (2.20). To this end, we consider the domain $\Omega = (-1, 1)^d$ with $d = 2, 3$, and the exact solution

$$u(x) = e^{-10\,|x|^2}$$

of (2.19) with $\mathbf{A} = \mathbf{I}$ and non-constant $f = -\Delta u$. Such an f exhibits a relatively large variation in Ω, and within elements, which forces AFEM to refine additional elements due to data oscillation (Marking Strategy O), not yet marked for refinement by Marking Strategy E. This is reported in Table 2.1 for two dimensions (left) and three dimensions (right). We see that the number of additional elements due to large data oscillation is rather small relative to those due to large error indicators, but it is *not* zero. On the one hand, this confirms that control of data oscillation cannot be omitted in a
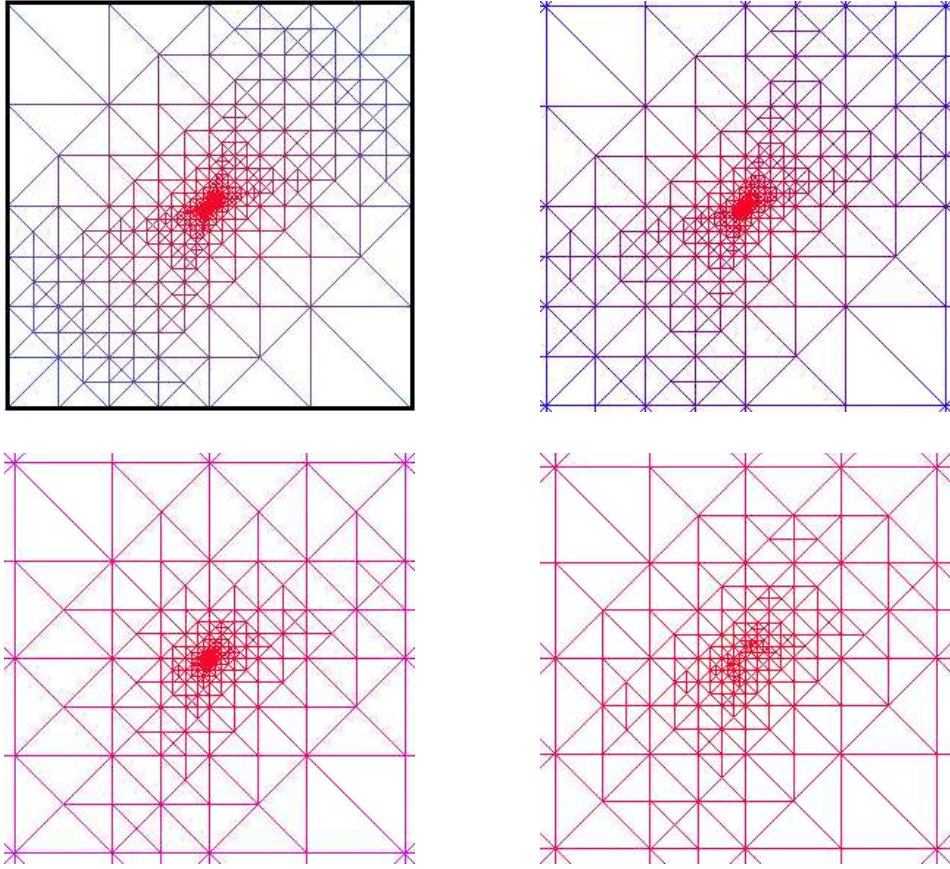
FIGURE 2.10. Example 2.6.1: Final grid (full grid with < 2000 nodes) (top left), zooms to $(-10^{-3}, 10^{-3})^2$ (top right), $(-10^{-6}, 10^{-6})^2$ (bottom left), and $(-10^{-9}, 10^{-9})^2$ (bottom right).
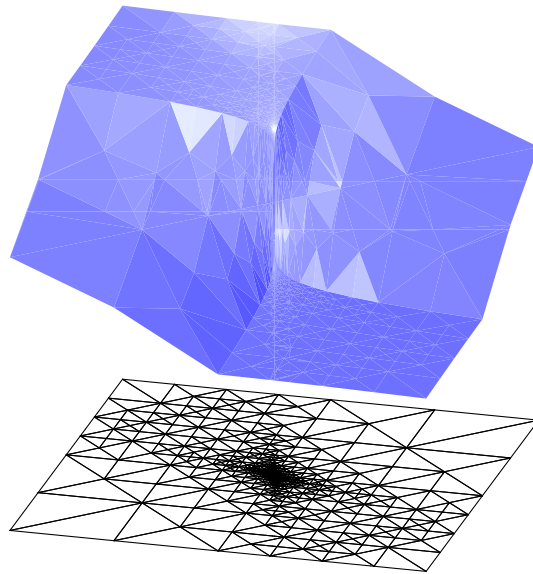

FIGURE 2.11. Example 2.6.1: Graph of the discrete solution, which is $\approx r^{0.1}$, and underlying grid.
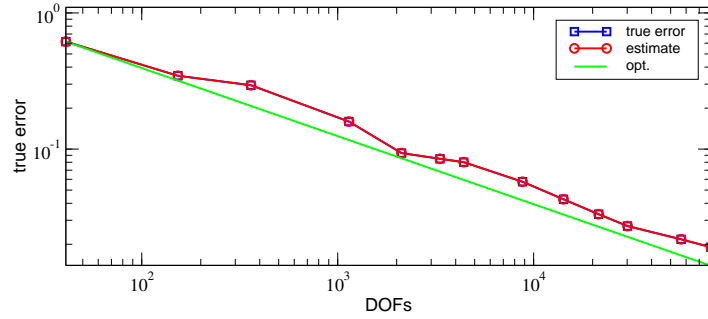
FIGURE 2.12. Example 2.6.2: Quasioptimality of AFEM: estimate and true error in two dimensions. The optimal decay is indicated by the green line with slope $-1/2$.
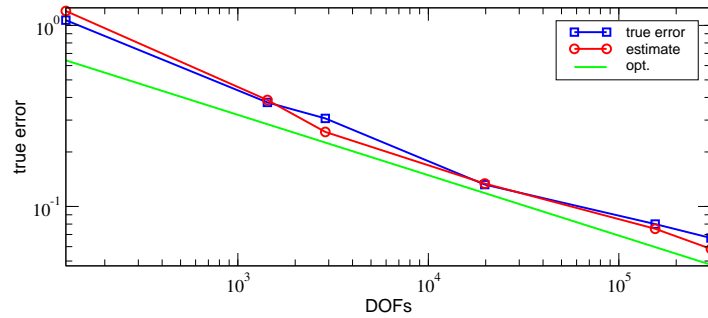

FIGURE 2.13. Example 2.6.2: Quasioptimality of AFEM: estimate and true error in three dimensions. The optimal decay is indicated by the green line with slope $-1/3$.

convergent algorithm. On the other hand, this explains why data oscillation seems to play a minor role for (piecewise) smooth data f, and hints at the underlying reasons why most adaptive strategies, although neglecting data oscillation, converge in practice.
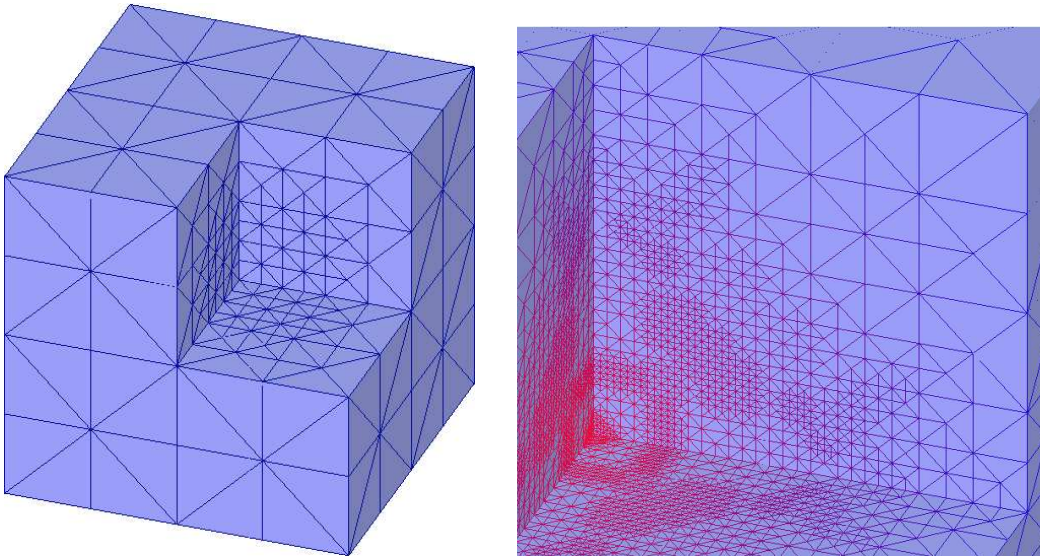

FIGURE 2.14. Example 2.6.2: Adaptive grids of the 3d simulation on $\partial((-1,1)^3 \backslash (0,1)^3)$: full grid of the 2nd iteration (left), zoom into the grid of the 4th iteration (right).

As mentioned in § 2.3, we produce in three dimensions the interior node by bisecting a marked tetrahedron six times. This corresponds in two dimensions to four bisections of a marked triangle, which is used here instead of the procedure of Figure 2.3. Although this produces more DOFs than needed, Figures 2.12 and 2.13 demonstrate that the resulting meshes are still quasi-optimal for both two dimensions and three dimensions. Here, the estimators η_k were scaled by the factor 0.25. For comparison with an optimal mesh, green lines with slope $-1/d$ are plotted in Figure 2.12 ($d = 2$) and Figure 2.13 ($d = 3$); note that these lines have nearly the same slope due to different scaling of the y axis.

Finally, in Figure 2.14 we cut $(0, 1)^3$ out of the domain $(-1, 1)^3$ and show the adaptive grid of the three-dimensional simulation on the boundary of the resulting domain. In the left picture we show the full grid of the 2nd iteration and in the right one a zoom into the grid of the 4th iteration. For this picture we also used the graphics package GRAPE.

2.7. Exercises.

2.7.1. *Exercise: Superconvergence.* Let $\mathcal{T}_h$ be a shape-regular triangulation of a polygonal domain $\Omega \subset \mathbb{R}^d$. Let $\mathbb{V}_h$ be a space of (possibly discontinuous) finite elements containing at least $\mathbb{P}_k(T)$ as interpolating polynomials for all $T \in \mathcal{T}_h$. Given $u \in L^2(\Omega)$ let $u_h \in \mathbb{V}_h$ be the L^2-projection of u onto $\mathbb{V}_h$, i.e.

$$u_h \in \mathbb{V}_h : \qquad \int_\Omega (u - u_h)v = 0 \quad \forall \, v \in \mathbb{V}_h.$$

Prove the following error estimates for $0 \le m \le k + 1$ ($H^{-m}(\Omega) =$ dual of $H_0^m(\Omega)$):

$$(2.26) \qquad \|u - u_h\|_{L^2(\Omega)} \le \inf_{v \in \mathbb{V}_h} \|u - v\|_{L^2(\Omega)} \le Ch^{k+1}|u|_{H^{k+1}(\Omega)};$$

$$(2.27) \qquad \|u - u_h\|_{H^{-m}(\Omega)} \le Ch^{k+1+m}|u|_{H^{k+1}(\Omega)};$$

$$(2.28) \qquad \|u - u_h\|_{H^m(\Omega)} \le Ch^{k+1-m}|u|_{H^{k+1}(\Omega)},$$

the latter provided $\mathcal{T}_h$ is quasi-uniform. The inequality (2.27) is referred to as a *superconvergence* estimate. Hint: to prove (2.28) add and subtract $I_h u$ and use an inverse inequality.

2.7.2. *Exercise: Equivalent Estimator.* Consider the *a posteriori* error estimator based only on jumps

$$\zeta_h = \Big(\sum_{S \in \mathcal{S}_h} h_S \|J_S\|_{L^2(S)}^2 \Big)^{1/2}.$$

The purpose of this problem is to demonstrate that ζ_h is equivalent to the true error $\|\nabla e_h\|_{L}^2(\Omega)$ under the same conditions that η_h is, where η_h is given by

$$\eta_h^2 = \sum_{T \in \mathcal{T}_h} h_T^2 \|f\|_{L^2(T)}^2 + \sum_{S \in \mathcal{S}_h} h_S \|J_S\|_{L^2(S)}^2.$$

(a) Let f_i be the L^2-projection of f onto the set of constants $\mathbb{P}_0(\omega_i)$ over the star $\omega_i = \mathrm{supp}(\phi_i)$. Use the error equation to deduce

$$\|f_i\|_{L^2(\omega_i)}^2 \le C\|f - f_i\|_{L^2(\omega_i)}^2 + C \sum_{S \ni \mathbf{x}_i} h_S^{-1} \|J_S\|_{L^2(S)}^2.$$

(b) Use that each triangle $T \in \mathcal{T}_h$ belongs to at most N sets ω_i with N independent of h to conclude that

$$\sum_{T \in \mathcal{T}_h} h_T^2 \|f\|_{L^2(T)}^2 \le Ch_{\max}^2 \sum_{1 \le i \le I} \|f - f_i\|_{L^2(\omega_i)}^2 + C \sum_{S \in \mathcal{S}_h} h_S \|J_S\|_{L^2(S)}^2.$$

(c) Show that

$$h_{\max}^2 \sum_{1 \le i \le I} \|f - f_i\|_{L^2(\omega_i)}^2 = o(h_{\max}^2),$$

and then prove that ζ_h is equivalent to $\|\nabla e_h\|_{L}^2(\Omega)$.

2.7.3. *Exercise: Data Oscillation.* Construct a counterexample with oscillatory function f showing that a global lower bound such as (2.7) cannot be valid without osc_H.

2.7.4. *Exercise: Data Oscillation Reduction 2.* Let f be piecewise H^s for $0 < s \leq 1$ over the initial mesh, where H^s stands for the space of functions with fractional derivative of order s in L^2. Let data oscillation be redefined by

$$\text{osc}_h := \left(\sum_{T \in \mathcal{T}_h} h_T^{2+2s} \|D^s f\|_{L^2(T)}^2 \right)^{1/2}.$$

Let γ_0, θ_0, and $\mathcal{T}_h$ be defined as in Lemma 2.10. If $\rho := (1 - (1 - \gamma_0^{2+2s})\theta_0^2)^{1/2}$, then show

$$(2.29) \qquad\qquad\qquad\qquad \text{osc}_h \leq \rho\, \text{osc}_H.$$

Since $\gamma_0 \leq 1/2$ in two dimensions, the reduction rate squared of is $\hat{\alpha}^2 \leq 1 - 15\hat{\theta}^2/16 \approx 1 - \hat{\theta}^2$ provided f is piecewise H^1.